Environmental Science & Technology

pubs.acs.org/est

Article

# $O_2$-Independent $H_2O_2$ Production via Water−Polymer Contact Electrification

Yanfeng Wang, Peiyun Wei, Zihan Shen, Chao Wang, Jie Ding,* Wenkai Zhang, Xin Jin, Chad D. Vecitis,* and Guandao Gao*

Cite This: *Environ. Sci. Technol.* 2024, 58, 925−934

Read Online

ACCESS | Metrics & More | Article Recommendations | Supporting Information

**ABSTRACT:** Hydrogen peroxide ($H_2O_2$), as a critical green chemical, has received immense attention in energy and environmental fields. The ability to produce $H_2O_2$ in earth-abundant water without relying on low solubility oxygen would be a sustainable and potentially economic process, applicable even to anaerobic microenvironments, such as groundwater treatment. However, the direct water to $H_2O_2$ process is currently hindered by low selectivity and low production rates. Herein, we report that poly(tetrafluoroethylene) (PTFE), a commonly used inert polymer, can act as an efficient triboelectric catalyst for $H_2O_2$ generation. For example, a high $H_2O_2$ production rate of 24.8 mmol $g_{cat}^{-1}$ $h^{-1}$ at a dosage of 0.01 g/L PTFE was achieved under the condition of pure water, ambient atmosphere, and no sacrificial agents, which exceeds the performance of state-of-the-art aqueous $H_2O_2$ powder catalysts. Electron spin resonance and isotope experiments provide strong evidence that water−PTFE tribocatalysis can directly oxidize water to produce $H_2O_2$ under both anaerobic and aerobic conditions, albeit with different synthetic pathways. This study demonstrates a potential strategy for green and effective tribocatalytic $H_2O_2$ production that may be particularly useful toward environmental applications.

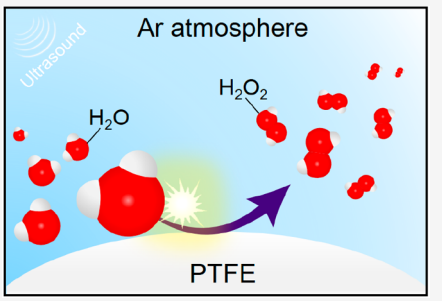


**KEYWORDS:** *hydrogen peroxide, water oxidation, tribocatalysis, ultrasound, polymer*



## INTRODUCTION

Hydrogen peroxide ($H_2O_2$), a green and ubiquitous chemical that can act as both an oxidant and a reductant, has been widely used in a variety of industries, such as organic synthesis, sterilization, electronics, paper/pulp bleaching, and environmental protection.[1−4] At present, the anthraquinone oxidation (AO) process is the dominant industrial technology for producing $H_2O_2$.[5] The AO process involves the sequential 2-electron redox reactions of hydrogenation and oxidation of the anthraquinone molecules, which requires a large energy input and generates a harmful organic waste byproduct.[6,7] Furthermore, long-distance transportation of concentrated reactive $H_2O_2$ imposes additional safety risks. Thus, the inherent complexity of the AO process has motivated many researchers toward development of direct in situ $H_2O_2$ synthesis methods with the ultimate goal of a green, efficient, modular, and continuous catalytic process.[2,5]

Photochemical (PC) and electrochemical (EC) $H_2O_2$ synthesis are sustainable and eco-friendly alternative technologies.[8−14] There are two mechanistic pathways to generate $H_2O_2$: one is by the reduction of molecular $O_2$, and the second less common pathway is by the oxidation of two water molecules. The reduction of oxygen for $H_2O_2$ generation ($O_2 + 2e^- + 2H^+ \rightarrow H_2O_2$; $E^\circ$ = 0.695 V vs SHE; pH 0) is energetically favorable as it involves no bond breaking, only the conversion of a O═O double bond to an O−O single bond along with the formation of two new H−O bonds. In stark contrast, the oxidation of two waters for $H_2O_2$ generation ($2H_2O \rightarrow H_2O_2 + 2e^- + 2H^+$; $E^\circ$ = 1.76 V vs SHE) is energetically unfavorable as it involves breaking of 2 H−O bonds along with formation of only 1 new O−O bond.[5] Although oxygen reduction is thermodynamically more favorable, the aqueous $H_2O_2$ production rate in ambient air is limited by the low solubility of oxygen in the normal conditions of temperature and pressure (~8 mg $L^{-1}$ or 250 $\mu$M). Methods such as aeration or pure $O_2$ sparging are able to maintain the $O_2$ concentration and enhance the $H_2O_2$ production rate; however, the oxygen utilization efficiency is low and aeration significantly increases the energy consumption.[15] There are also cases where anaerobic conditions would render classical reductive $H_2O_2$ generation negligible, such as groundwater treatment.

Water oxidation is a potential alternative to oxygen reduction for producing $H_2O_2$.[16,17] A primary hurdle to producing $H_2O_2$ via water oxidation is that the four electron

Received: September 18, 2023
Revised: November 21, 2023
Accepted: November 27, 2023
Published: December 20, 2023

oxidation of water to oxygen ($2H_2O \rightarrow O_2 + 4e^- + 4H^+$; $E^\circ$ = 1.23 vs SHE) has a lower energetic barrier than the two electron water oxidation to $H_2O_2$.[17] Additionally, a superior two electron water oxidation catalyst must also satisfy other criteria such as robust stability for long-term operation, exceptional selectivity to avoid byproducts formation and high activity to reduce energy consumption.[18] Thus, not only is there a large thermodynamic barrier to oxidative $H_2O_2$ synthesis, but the reactants also need to be locally limited to prevent continued $H_2O_2$ oxidation to HOO• or $O_2$.[16,19] Due to these energetic and mechanistic difficulties, there is a long path toward the selective oxidation of water for $H_2O_2$ synthesis due to the energy requirements and low yield and selectivity.[20−23]

Triboelectric and/or piezoelectric particles have been reported to have utility toward a range of processes including organic synthesis, energy generation, and environmental control.[24−27] For example, triboelectric effects at the liquid−hydrophobic material interface can generate surface potentials up to ∼100 V, which can drive the ionization of liquid water ($H_2O \rightarrow H_2O^+ + e^-$) potentially initiating a radical chain reaction process to form •OH (e.g., $H_2O^+ + H_2O \rightarrow$ •OH + $H_3O^+$),[28,29] then combine with each other to produce $H_2O_2$. Such high surface voltage in the triboelectric process can easily trigger a variety of strong oxidation and reduction reactions. This presents a noteworthy advantage as compared to the photocatalytic or electrocatalytic process, where even the state-of-the-art metal oxide catalysts still require more than 1 V overpotential from the equilibrium potential for $H_2O_2$ (1.76 V vs RHE).[18] Moreover, most hydrophobic material contact-electrification-induced electrons can directly mediate the catalytic process. On the contrary, the catalysts selected for two electron water oxidation are highly dependent on the binding energy of oxygen intermediates (*O, *OH, and *OOH) and the catalysts.[30] Thus, tribocatalytic water decomposition may be a potential alternative to classical methods for peroxide production. However, this novel $H_2O_2$ generation process is immature, with few studies focused on reaction design optimization and/or synthetic mechanisms and kinetics.

Here, we report that the classically inert organic polymer polytetrafluoroethylene (PTFE) can be effectively and efficiently utilized as a triboelectric catalyst for oxygen-independent $H_2O_2$ production. The tribocatalytic process is induced by ultrasound irradiation of PTFE microparticles−water, resulting in a maximum $H_2O_2$ production rate of 24.8 mmol $g_{cat}^{-1}$ $h^{-1}$ at a dosage of 0.01 g/L PTFE that greatly surpasses state-of-the-art photocatalytic and piezocatalytic $H_2O_2$ production systems. The PTFE catalyst has the advantages of operating under STP conditions, in the absence of scavengers and in the absence of air (i.e., abundant water was the only reactant). The fundamental $H_2O_2$ production mechanisms and potential tribocatalytic applications were also investigated.

## MATERIALS AND METHODS

**Materials and Reagents.** PTFE powders (⟨d⟩ ∼ 1−5 μm) and potassium titanium(IV) oxalate were supplied by Macklin. Polypropylene (PP, average 5 μm) and fluorinated ethylene propylene (FEP, average 10 μm) were purchased from Dongguan Tesulang Chemical Chemical Co., Ltd. 5,5-Dimethyl-1-pyrolin-N-oxide (DMPO) was purchased from Dojindo Laboratories (Japan). 2,2,6,6-Tetramethyl-4-piperidinol (TEMP) and dimethyl sulfoxide (DMSO) were purchased from Sigma-Aldrich (U.S.A). Titanium dioxide ($TiO_2$), water-$^{18}O$ (97 atom %), and boron nitride (BN) were purchased from Aladdin Chemistry Co., Ltd. 4-Carboxyphenylboronic acid was obtained from Shanghai Yuanye Bio-Technology Co., Ltd., Shanghai, China. Calcium chloride ($CaCl_2$), calcium nitrate ($Ca(NO_3)_2$), sodium chloride (NaCl), magnesium nitrate ($Mg(NO_3)_2$), magnesium chloride ($MgCl_2$), aluminum chloride ($AlCl_3$), zinc chloride ($ZnCl_2$), sodium sulfate ($Na_2SO_4$), sodium carbonate ($Na_2CO_3$), sodium phosphate ($Na_3PO_4$), and glucose were purchased from Sinopharm Chemical Reagent Co. Ltd., Shanghai, China.

**Experimental Procedure.** *Qualitative Characterization of $H_2O_2$ Production by PTFE.* Here, 0.1 g/L PTFE (0.1 g/L) and 50 mL of deionized water were exposed to ultrasound irradiation for 1 h. Then, the 1 mg/L 4-carboxyphenylboronic acid was added to the above reacted solution containing $H_2O_2$. After mixing for 0.5 h, 1 mL of mixture solution was injected into the high resolution Q Exactive Focus Orbitrap tandem mass spectrometer (Thermo Fisher Scientific Inc., Germany).

*Quantitative Characterization of $H_2O_2$ Production by PTFE.* The standard reaction conditions for $H_2O_2$ generation were pure water and an ambient atmosphere. A certain amount of PTFE and 50 mL of deionized water were placed in a 100 mL breaker. The pH was adjusted with 1 M dilute $H_2SO_4$ or NaOH. The mixture was exposed to ultrasound irradiation with a frequency of 40 kHz in an ultrasound cleaner (Branson 3800-CPXH). At time intervals, 1 mL of sample was centrifuged to remove PTFE particles and analyzed by potassium titanium(IV) oxalate to determine the concentration of $H_2O_2$. In detail, to prepare the potassium titanium(IV) oxalate reagent, 7.083 g of potassium titanium(IV) oxalate reagent was dissolved in 136 mL of 98% $H_2SO_4$ and 114 mL of deionized water. Here, 0.5 mL of sample and 0.5 mL of potassium titanium(IV) oxalate reagent were placed in a 10 mL colorimetric tube then made up to 5 mL. The mixture solution was measured using UV−vis spectrophotometer (Shimadzu, UV-1800) at 400 nm. The concentration of $H_2O_2$ was calculated by the equation given in Figure S1. The correlation coefficient is very high ($R^2$ = 0.9989), which means the work curve is accurate and reliable.

*Isotope Experiments.* Here, 0.1 g/L of PTFE, 1 mL of $H_2{}^{18}O$ (97 atom %), and 20 μL of 50 mg/L of benzoic acid were placed in a 10 mL breaker. The mixture was exposed to ultrasound irradiation in the ultrasound cleaner. After ultrasound for 30 min, the mixture solution containing *p*-HBA, *o*-HBA, and *m*-HBA was analyzed by Dionex Ultimate 3000 ultrahigh performance liquid chromatography (UHPLC) system coupled with a high resolution Q Exactive Focus Orbitrap tandem mass spectrometer. Chromatographic separation was carried out with a C18 column (2.1 mm × 100 mm, 1.8 μm; Agilent Technologies, USA). The mobile phase A was 0.1% formic acid in $H_2O$, and B was MeOH. The program was as follows: 0−12 min, 60% A, 40% B. The flow rate was 0.2 mL/min, and the injection volume was 10 μL.

The qualitative characterization of hydroxybenzoic acids with the molecular formulas $C_7H_5{}^{16}O_2{}^{18}O$ and $C_7H_5{}^{16}O_3$ were performed under negative heated electrospray-ionization ($HESI^-$). The HESI spray voltage was −3.0 kV. The capillary temperature and probe heater temperature were 350 and 450 °C, respectively. The sheath gas, auxiliary gas, and sweep gas were 35 (arbitrary units), 10 (arbitrary units), and 1 (arbitrary units), respectively.


https://doi.org/10.1021/acs.est.3c07674
Environ. Sci. Technol. 2024, 58, 925−934

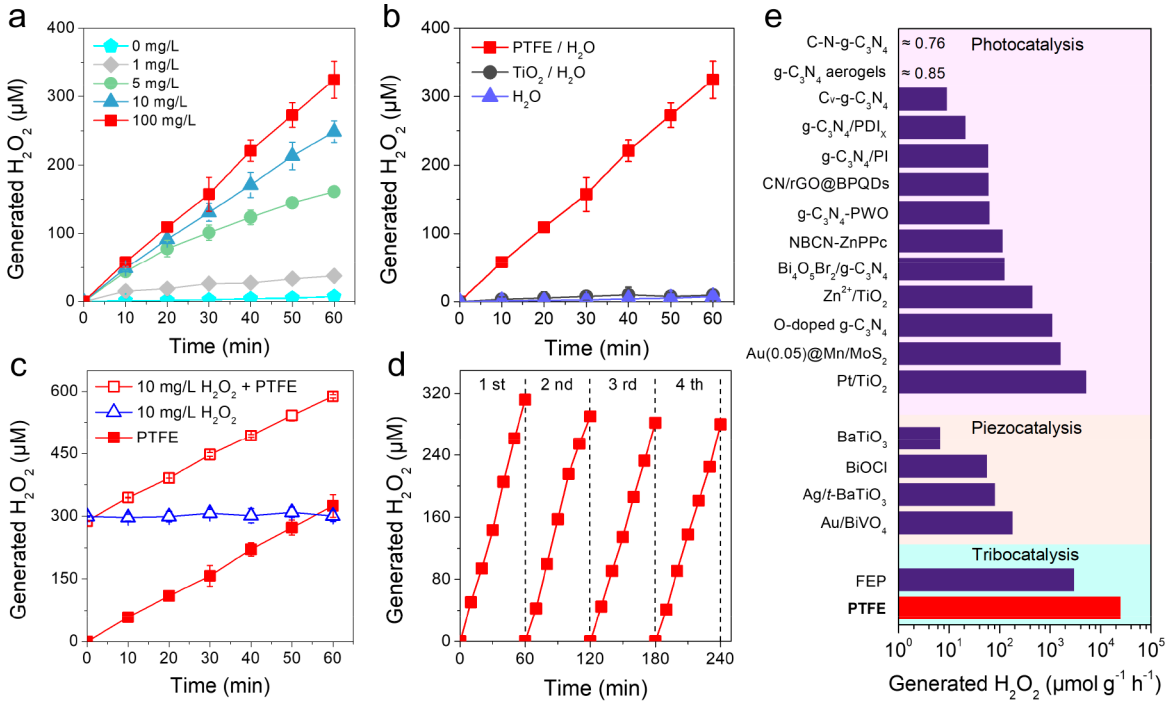


**Figure 1.** Ultrasonic $H_2O_2$ generation was carried out by PTFE. (a) Effect of PTFE concentration on $H_2O_2$ generation. (b) Comparison of ultrasonic production of $H_2O_2$ between PTFE and $TiO_2$ $[Catalyst]_0$ = 0.1 g/L. (c) Changes in the $H_2O_2$ concentration during the ultrasonic process over time. Blue points show the results of ultrasound irradiation with water containing ca. 10 mg/L of $H_2O_2$. (d) Cycling runs for $H_2O_2$ generation over PTFE. (e) Comparison of $H_2O_2$ generation with photocatalysis and piezocatalysis; for detailed information, see Tables S1 and S2. $[PTFE]_0$ = 0.01 g/L.

*Reactive Oxygen Species (ROS) Generation by PTFE.* Electron spin resonance (ESR) was recorded on a Bruker EMX-10/12 spectrometer (Germany). Hydroxyl radicals (•OH) were trapped by DMPO. Superoxide radical ($•O_2^-$) was trapped by DMPO/DMSO. The reactions were carried out in 1.5 mL centrifuge tubes with 0.5 mL of deionized water containing 4 g/L of PTFE and 100 mM DMPO to detect DMPO-•OH by ESR. Deionized water (0.5 mL) containing 4 g/L of PTFE, 100 mM DMPO, and 1 M DMSO were employed to detect DMPO/DMSO-$•O_2^-$ by ESR. After 10 min of ultrasonic irradiation in the ultrasonic cleaner, the solutions were analyzed by ESR. In the Ar atmosphere, the deionized water was deoxygenated by bubbling Ar gas for 30 min before ultrasonic irradiation. During the reaction, the mixture was continuously purged with Ar.

*Computational Details.* Density functional theory (DFT) calculations were employed using the Dmol$^3$ code,[31] with the Generalized Gradient Approximation (GGA) and PBE functionality[32] utilized to handle exchange-related interactions. A double numerical quality basis set with d-type polarization functions[33] (DNP) was used for all geometry optimizations and total energy calculations, while effective core pseudopotentials (ECP)[34,35] were utilized to model core electrons. All calculations were spin-unconstrained. To simulate a solvent environment, a conductorlike screening model (COSMO) was employed with a dielectric constant of 78.54. The positions of all atoms were fully relaxed until the following convergence criteria were met: force of 0.002 Ha/Å, total energy of $10^{-5}$ Ha, and displacement of 0.005 Å. The actual space cutoff radius was 4.1 Å, and the self-consistent field calculation standard was selected as $10^{-6}$ Ha. The calculations considered the elastic compression of PTFE particles with a compression ratio.[27]

Further details about the DFT calculations can be found in a previous study.[27] Generally, the pressure induced by cavitation bubbles is around 100 MPa, which may cause a 30% compressive ratio of PTFE. It is also assumed that the compression occurs along the folding direction of the PTFE molecular chains. Consequently, the compression of volume from 10 Å × 10 Å × 5 Å to 10 Å× 7 Å × 5 Å is considered equivalent to the high-pressure environment induced by the collapse of cavitation bubbles.

## RESULTS AND DISSCUSSION

**Confirmation and Quantification of $H_2O_2$ Generation by Water−PTFE Contact Electrification Catalysis.** The $H_2O_2$ generation by the ultrasonic irradiation of PTFE was confirmed by the cleavage of 4-carboxyphenylboronic acid, an $H_2O_2$ specific reagent (Figure S2).[36,37] Next, potassium titanium oxalate (PTO) was used to quantitatively analyze the production of $H_2O_2$ as a function of time as displayed in Figure 1a with data at all PTFE concentrations having zero-order kinetics.[38] As the PTFE catalyst concentration increases from 1 to 100 mg/L, the concentration of $H_2O_2$ after 60 min of irradiation increased from 37.8 ± 5.2 to 324.8 ± 27.2 μM. Ultrasonic irradiation of $TiO_2$ and pure water was completed as control experiments as displayed in Figure 1b, and both had negligible production of $H_2O_2$ (<10 μM) after 60 min. This result indicates that ultrasonic irradiation of PTFE particles was the predominant mechanism for the $H_2O_2$ production in this system. Ultrasonic waves can drive the nucleation, growth, and collapse of cavitation bubbles in the aqueous solutions that generates extremely high temperatures and pressures, which in


https://doi.org/10.1021/acs.est.3c07674
Environ. Sci. Technol. 2024, 58, 925−934

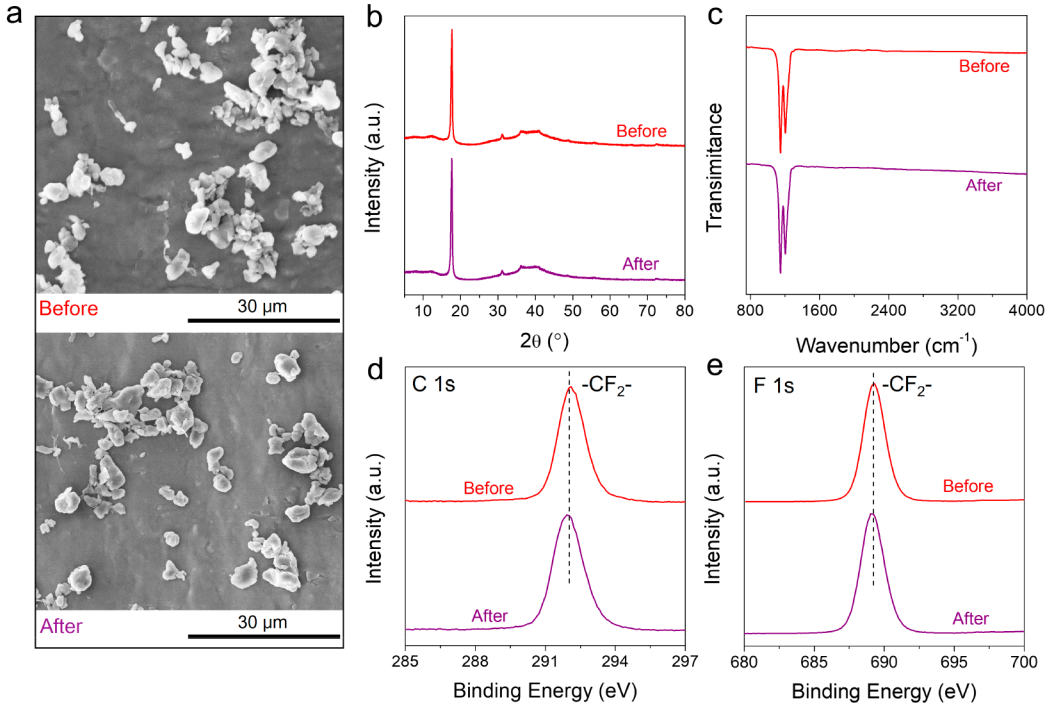


**Figure 2.** Characterization of PTFE before and after reaction. (a) SEM, (b) XRD, (c) FT-IR spectrum, and (d, e) XPS of PTFE before and after ultrasound.

turn may produce highly reactive free radicals (e.g., HO•) and $H_2O_2$.[39] However, the low ultrasonic power intensity (~0.3 W/cm$^2$) used here was insufficient to drive these processes resulting in negligible $H_2O_2$ generation in the pure water control.

Next, we investigated the stability of the generated $H_2O_2$. We carried out two comparative experiments, in which two beakers containing 50 mL of 10 mg/L of $H_2O_2$ and 10 mg/L of $H_2O_2$ + PTFE were separately ultrasonically irradiated (Figure 1c). After ultrasonication for 1 h, essentially no difference in the $H_2O_2$ concentration was observed, suggesting that $H_2O_2$ is not decomposed by ultrasonic irradiation alone under our experimental conditions and steady-state PTFE catalysis results in a linear increase in $H_2O_2$ concentration within 10 h of ultrasound (Figure S3). Notably, the formation and decomposition of $H_2O_2$ during most catalytic processes proceed concurrently and competitively. For example, photocatalytically produced $H_2O_2$ may also be decomposed by its reaction with both conduction band (CB) electrons and the valence band (VB) holes into a variety of species such as $H_2O$, •OH, •$HO_2$, and $O_2$.[1,40] However, the decomposition of $H_2O_2$ did not occur in the PTFE catalysis system, suggesting that catalytic $H_2O_2$ generation in the PTFE system is likely due to an alternative synthesis mechanism.

The PTFE catalytic stability was examined by completion of recycle experiments (Figure 1d). The PTFE was recovered by vacuum filtration onto a filter membrane and resuspended to produce $H_2O_2$ under the same conditions. The results indicate that there was a slight reduction in $H_2O_2$ production after reuse, as a result of PTFE particle loss during the catalyst recycling process. After the fourth recycle, the concentration of $H_2O_2$ after 1 h of irradiation was around 280 $\mu$M, indicating the PTFE still had good catalytic activity. Scanning electron microscopy (SEM), X-ray diffraction (XRD), Fourier transform infrared (FT-IR) spectroscopy, and X-ray photoelectron spectroscopy (XPS) revealed that there was no change in the PTFE morphology or chemical composition after ultrasonication (Figure 2). These data confirmed the chemical stability of PTFE and that PTFE acted as a $H_2O_2$ generation catalyst.

Current technologies for using powder materials to catalyze the production of $H_2O_2$ primarily involve piezocatalysis and photocatalysis. Although piezocatalysis has received widespread attention in energy harvesting, environmental remediation, and ROS generation, there is less literature focused directly on $H_2O_2$ production. As compared with state-of-the-art piezocatalysts, PTFE displays orders of magnitude higher $H_2O_2$ production rates (Figure 1e). In addition, photocatalytic $H_2O_2$ production often requires sacrificial electron donors such as small organic acids/alcohols or alternative reduced species to consume photogenerated holes to prevent $H_2O_2$ degradation and to inhibit the recombination of photogenerated carriers. Electron donor addition is an effective way to increase $H_2O_2$ production, but may contaminate the produced $H_2O_2$ and will increase operating cost.[8] Thus, here, we compared $H_2O_2$ production between common photocatalysts and PTFE catalysts in the absence of sacrificial electron donors. As displayed in Figure 1e, the comparison suggests that the PTFE performance is, to a large extent, superior to all reported photocatalysts and piezocatalysts under similar conditions (i.e., ambient atmosphere, room temperature, pure water). In addition, to the best of our knowledge, PTFE is comparable to the best photocatalysts used in a pure oxygen atmosphere (Table S3). Moreover, there are reports on water-fluorinated ethylene propylene (FEP) tribocatalysis for $H_2O_2$ production this year.[41] However, the performance of FEP remains inferior to PTFE.

**Mechanism of $H_2O_2$ Formation in the Water−PTFE Tribocatalytic System.** The rapid $H_2O_2$ production in the water−PTFE tribocatalytic system may arise from a unique


https://doi.org/10.1021/acs.est.3c07674
Environ. Sci. Technol. 2024, 58, 925−934

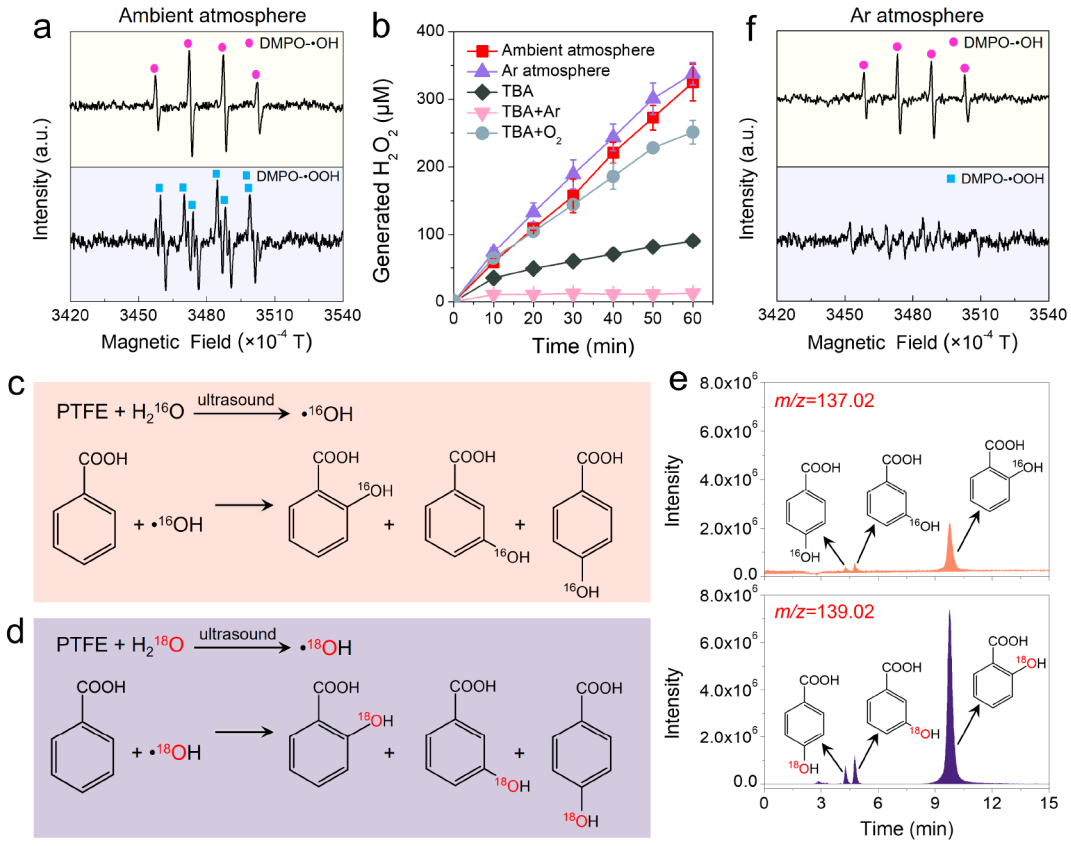


**Figure 3.** Water oxidation and oxygen reduction generate $H_2O_2$ over PTFE. (a) ESR signals for DMPO-•OH and DMPO-•OOH under ambient atmosphere. (b) Effect of scavengers on the amount of $H_2O_2$ generation (100 mM TBA). Reaction schemes of (c) $\bullet^{16}OH$ and (d) $\bullet^{18}OH$ with BA. (e) Total ion chromatogram of $\bullet^{16}OH$ and $\bullet^{18}OH$ reacted with BA. (f) ESR signals for DMPO-•OH and DMPO-•OOH under an Ar atmosphere.

and novel mechanism. Therefore, we investigated all possible pathways for its formation. The hydrogen atoms in produced $H_2O_2$ must come from water, but the oxygen atom source may be either from water oxidation or atmospheric $O_2$ reduction. There are two possible pathways for $H_2O$ oxidation into $H_2O_2$: a concerted $2e^-$ transfer from two adjacent $H_2O$ (eq 1) and two $1e^-$ transfers from two different $H_2O$ (eq 3) followed by radical recombination (eq 4).[42,43] The DMPO spin-trapping ESR technique was employed to identify the production of •OH, thereby verifying the possible oxidation pathways from $H_2O$ to $H_2O_2$. Figure 3a clearly shows the detection of quadruplet DMPO-•OH peaks in the ultrasound-PTFE system. Furthermore, *tert*-butyl alcohol (TBA) was used as an •OH scavenger and the addition of TBA depressed (>70%) $H_2O_2$ generation from 324.8 ± 27.2 to 90.5 ± 2.5 $\mu$M after 1 h of ultrasonication (Figure 3b), indicating that •OH played a key role in the $H_2O_2$ generation. The pH also decreased from 5.6 to 3.6 after 4 h of ultrasound irradiation (Figure S4), which was probably attributed to generation of •OH and $H^+$ during water oxidation (eq 3).

Additional isotope experiments were performed to explore whether •OH resulted from water oxidation. In these experiments, benzoic acid (BA) is used as probe for •OH;[44] this reaction produces *para*-hydroxybenzoic acid (*p*-HBA) as well as *ortho*- (*o*-HBA) and *meta*- (*m*-HBA) (Figure 3c). The $H_2{}^{18}O$ + PTFE system was used for ultrasonic production of $\bullet^{18}OH$. If water oxidation is the origin of •OH in the $H_2O_2$ production, hydroxybenzoic acid with the molecular formula $C_7H_5{}^{16}O_2{}^{18}O$ would be detected, as shown in Figure 3d. According to the results of LC-MS, the mass spectrometric peaks at 137.02 and 139.02 obtained in the $H_2{}^{16}O$ and $H_2{}^{18}O$/PTFE/BA systems (Figure 3e, Figure S5) indicated that •OH generation originated from water oxidation.

However, $H_2O_2$ production was not completely inhibited even at a high TBA (200 mM) concentration (Figure S6), suggesting that the recombination of •OH from water oxidation was not the only pathway for $H_2O_2$ production in the ultrasound-PTFE system. The ESR results also showed PTFE catalysis yielded DMPO/DMSO-•OOH peaks, as displayed in Figure 3a, which is generated as an intermediate in the $1e^-$ reduction of $O_2$ (eq 5). The superoxide radicals can subsequently contribute to $H_2O_2$ production via the superoxide dismutation reaction pathway (eqs 6–8).[43,45] Therefore, it seems reasonable to conclude that $1e^-$ oxygen reduction is also occurring in the ultrasound-PTFE system, especially since water oxidation would need to be paired with a reductive process to conserve electroneutrality. Indeed, we found that changing from an ambient atmosphere to pure $O_2$ increased the $H_2O_2$ yield from 90.46 ± 2.52 to 251.44 ± 17.25 $\mu$M in the presence of •OH scavenger TBA (Figure 3b). Moreover, bubbling Ar in the TBA solution nearly completely suppressed $H_2O_2$ yield, indicating dissolved $O_2$ as a reactant under an ambient atmosphere and oxidative $H_2O_2$ production did not occur via a concerted $2e^-$ water oxidation pathway (eq 1).

$$2H_2O \rightarrow H_2O_2 + 2H^+ + 2e^- \quad E^\circ = 1.76\,V \text{ vs SHE} \tag{1}$$

$$2H_2O \rightarrow O_2 + 4H^+ + 4e^- \quad E^\circ = 1.23\,V \text{ vs SHE} \tag{2}$$



https://doi.org/10.1021/acs.est.3c07674
Environ. Sci. Technol. 2024, 58, 925−934

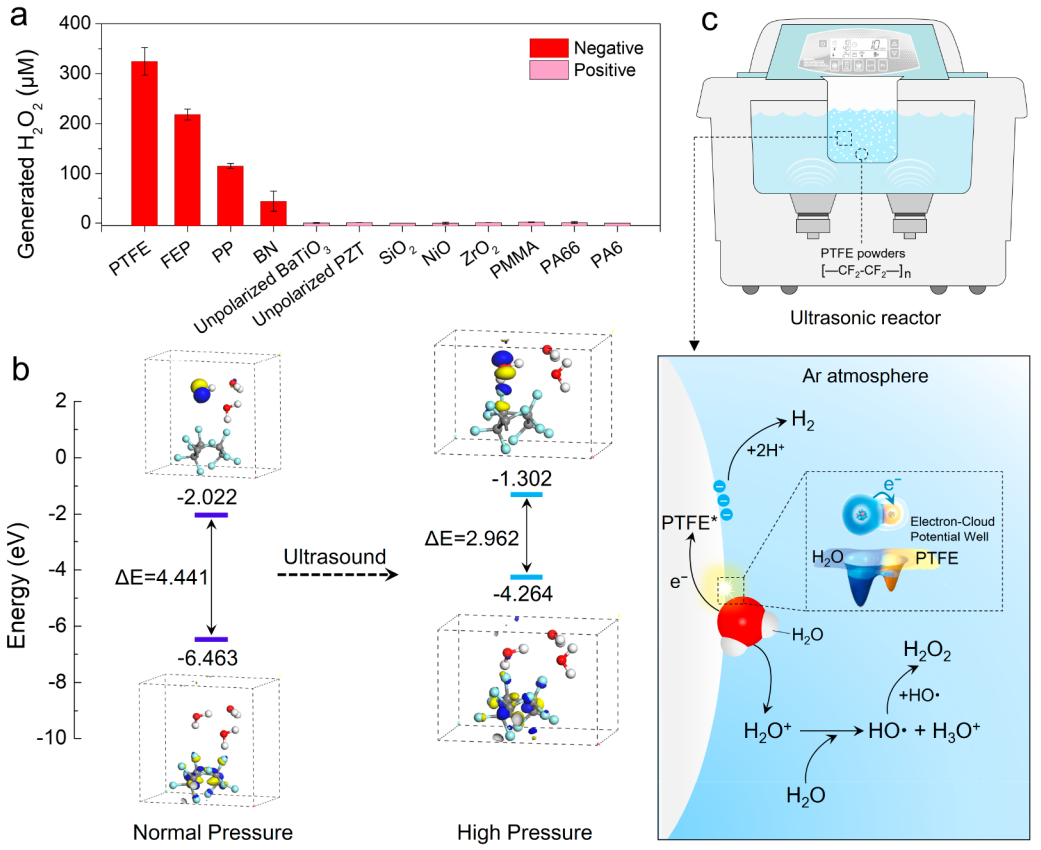


**Figure 4.** Mechanism of $H_2O_2$ production over PTFE. (a) Comparison of the $H_2O_2$ generation produced by different materials. $[Catalyst]_0$ = 0.1 g/L. (b) DFT calculations of the values of LUMO and HOMO levels for water−PTFE contact. (c) Schematic representing the $H_2O_2$ generation via the water−PTFE triboelectric process in the Ar atmosphere.

$$H_2O \rightarrow {}^{\bullet}OH + H^+ + e^- \quad E^\circ = 2.80\,V\ vs\ SHE \tag{3}$$

$${}^{\bullet}OH + {}^{\bullet}OH \rightarrow H_2O_2 \quad 5.2 \times 10^9\,M^{-1}s^{-1} \tag{4}$$

$$O_2 + e^- \rightarrow {}^{\bullet}O_2^- \quad 1.9 \times 10^{10}\,M^{-1}s^{-1} \tag{5}$$

$${}^{\bullet}O_2^- + H^+ \rightarrow HO_2\bullet \quad pK_a = 4.8 \tag{6}$$

$${}^{\bullet}O_2^- + HO_2\bullet \rightarrow HO_2^- + O_2 \quad 9.7 \times 10^7\,M^{-1}s^{-1} \tag{7}$$

$$HO_2^- + H^+ \rightarrow H_2O_2 \quad pK_a = 11.6 \tag{8}$$

$${}^{\bullet}OH + {}^{\bullet}HO_2 \rightarrow H_2O + O_2 \quad 7.1 \times 10^9\,M^{-1}s^{-1} \tag{9}$$

Interestingly, in the absence of TBA, bubbling Ar in a pure water solution slightly increased $H_2O_2$ yield (337.7 ± 16.4 μM) as compared to that in ambient atmosphere (Figure 3b). ESR confirmed that •OH was the primary reactive oxygen species, while $•O_2^-$ was below the limit of detection (Figure 3f). These data indicate that the PTFE ultrasonication primarily oxidized water to •OH (eq 3), and •OH was the dominant contributor to $H_2O_2$ formation (eq 4). Since •OH also acts as scavengers of $O_2$ reduction intermediates $•O_2^-$ and $HO_2•$ (eq 9), the $H_2O_2$ yield under an Ar atmosphere is higher than that under ambient atmosphere. Bubbling pure $O_2$ led to a clear decrease in the $H_2O_2$ yield (Figure S7), supporting the hypothesis that $O_2$ reduction intermediates were scavenging •OH. Additionally, considering that oxygen is the primary electron acceptor in the ambient atmosphere, $•O_2^-$ and $H_2O_2$ generated via superoxide dismutation reaction pathways could be detected. In contrast, in the Ar atmosphere, protons are the only possible electron acceptors, and their reduction would result in the formation of $H_2$ (Figure S8).

In summary, PTFE ultrasonication can directly catalyze water oxidation to produce $H_2O_2$ in the absence of $O_2$, which is of great benefit under certain circumstances, such as the hypoxic environment found in wastewater. Ultimately, a high $H_2O_2$ production rate can be obtained in the ultrasound-PTFE system under both anaerobic and aerobic conditions, and the dominant $H_2O_2$ production mechanism is oxygen independent.

**Mechanism of Charge Carrier Formation in the Water−TFE Tribocatalytic System.** Now that the chemical reaction mechanisms resulting in $H_2O_2$ production have been identified, the question remains of how the initial charge carriers are created during PTFE ultrasonication. The mechanism for charge carrier generation during catalytic PTFE ultrasonication is not presently clear, and a triboelectric effect is the likely candidate. It has been demonstrated that the friction reaction between PTFE and a semiconductor can achieve environmental pollutant degradation.[46] Previous reports have also shown that polymers, especially PTFE, can withdraw electrons from water during the liquid−solid contact electrification process.[28,47,48] That is, ultrasound can drive the rapid and large radial oscillation of bubble radii,[49] and any PTFE particles attached to the bubble will undergo similar stretching and contraction cycles. The viscous friction generated between the PTFE and water during these cycles may cause the electron clouds of PTFE and $H_2O$ to overlap and reduce the potential barrier.[50] This leads to the transfer of


https://doi.org/10.1021/acs.est.3c07674
Environ. Sci. Technol. 2024, 58, 925−934

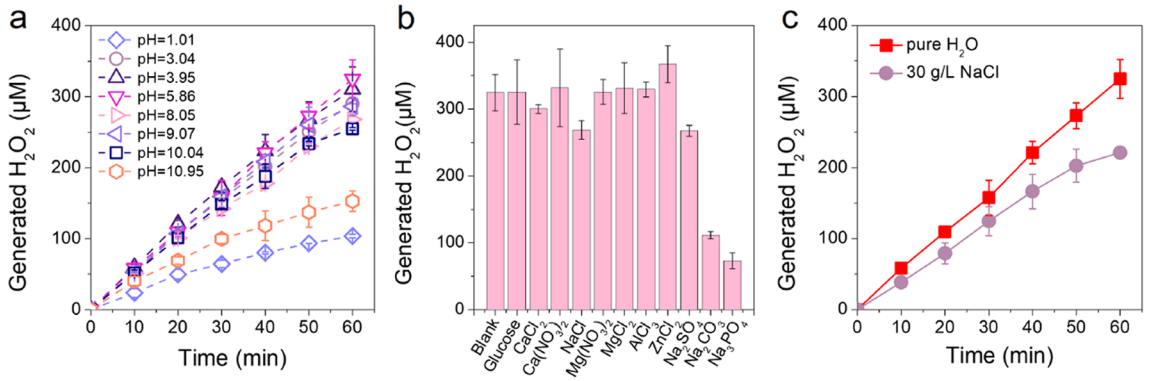


**Figure 5.** Potential application of $H_2O_2$ generation by PTFE. (a) $H_2O_2$ generation at different pH values. (b) Effect of inorganic (0.5 g/L) and organic matters (1 g/L) on the activity of PTFE toward $H_2O_2$ generation. (c) Time courses of $H_2O_2$ production by PTFE under ultrasound of saturated NaCl aqueous solution. $[PTFE]_0$ = 0.1 g/L.

an electron from the water molecule to the highly electronegative PTFE fluorine, yielding $PTFE^- + H_2O^+$. Immediately, the $H_2O^+$ reacts with a neighboring water molecule to yield an •OH and $H_3O^+$ ($H_2O^+ + H_2O \rightarrow$ •OH + $H_3O^+$).[29,51,52] Subsequently, two •OH can be combined into $H_2O_2$ as in eq 4.

To gain a better understanding of the charge carrier generation mechanism, materials of varying polarity were evaluated for $H_2O_2$ generation performance (Figure 4a). Negative triboelectric materials such as PTFE, fluorinated ethylene propylene (FEP), polypropylene (PP), and boron nitride (BN) displayed greater $H_2O_2$ generation performance, while positive triboelectric materials had poor $H_2O_2$ generation performance. Since higher negative triboelectric materials have stronger electron-withdrawing ability than positive triboelectric materials,[53,54] the electrons were more easily transferred from water molecules to negative triboelectric materials during contact electrification process that then drives the water oxidation reaction. In contrast, it is difficult for materials with positive triboelectricity to obtain electrons from water, which leads to poor catalytic performance. Our experiments showed that water−polymer contact electrification could be used to generate $H_2O_2$ universally. However, further research is needed to examine the impact of the polymer's microstructure, hydrophilicity, and particle size on its contact electrification performance.

Furthermore, density functional theory (DFT) calculations were employed to investigate the process of electron transfer between PTFE and water. Our theoretical calculations showed an energy band gap of 4.441 eV between LUMO and HOMO under normal pressure. When ultrasonic irradiation was applied, the energy barriers were significantly lowered to 2.962 eV, as illustrated in Figure 4b. This reduction in energy barriers was observed to facilitate the electron transfer between PTFE and water and thus promote the catalytic production of $H_2O_2$. Based on this finding and the aforementioned discussion, we propose a triboelectric mechanism for the PTFE-catalyzed production of $H_2O_2$ (Figure 4c). Specifically, we suggest that ultrasound induces friction between PTFE and water molecules, leading to the loss of an electron from water and the formation of an aqueous •OH, and then, two •OH combine to form $H_2O_2$.

**Potential Practical Application of $H_2O_2$ Generation by PTFE.** In summary, the PTFE catalyzed $H_2O_2$ yield was as high as 24.8 mmol $g_{cat}^{-1}$ $h^{-1}$ at a dosage of 0.01 g/L in an ambient atmosphere (STP with no sacrificial electron donor) after ultrasonication for 1 h. This inspired us to further investigate the potential of PTFE in practical applications over a range of aqueous conditions (e.g., pH and specific ions) on catalytic activity toward $H_2O_2$ generation. There was minimal change in $H_2O_2$ production (290.1 ± 0.4 μM) under weakly acidic conditions (pH 3.04) as displayed in Figure 5a. However, only 103.7 ± 2.6 μM $H_2O_2$ was generated at pH 1.01 since excessive $H^+$ would also compete with $O_2$ for produced $e^-$ and inhibit the •OH production according to eq 3 and Le Chatelier's Principle. There was a slight decrease in $H_2O_2$ production (254.72 ± 1.68 μM) upon increasing the pH to 10. $OH^-$ is a hole scavenger forming •OH that can generate $H_2O_2$ via •OH recombination.[14] On the other hand, increasing pH will inhibit superoxide/hydroperoxy dismutation to $H_2O_2$ that requires at least 1 hydroperoxy radical (eqs 5−8; $pK_a$ = 4.8) as observed in Figure 5a. The $H_2O_2$ produced decreased by nearly two times when the pH increased to 11 due to approaching the $pK_a$ of eq 8 and the formation of reactive $HO_2^-$. Thus, $H_2O_2$ production by PTFE ultrasonication can occur under weakly acidic, neutral, or weakly alkaline conditions (pH 3−10) common to biological and environmental systems, which is advantageous for practical applications.

In addition, we found that the addition of common ions, such as $Na^+$, $Mg^{2+}$, $Al^{3+}$, $Zn^{2+}$, $Cl^-$, and $NO_3^-$, had no significant effect on the $H_2O_2$ generation (Figure 5b). The amount of $H_2O_2$ generation for a wide range of common ions achieved 260−370 μM after 1 h of irradiation. However, $H_2O_2$ yield decreased when adding $CO_3^{2-}$, $SO_4^{2-}$, and $PO_4^{3-}$, which may be attributed to the fact that these anions can act as •OH scavengers.[55,56] The increase of solution negative charges can also hinder electron transfer between a water molecule and a PTFE particle[57] and results suggest that to be the dominant effect here. Additional studies also established the limited effect of organic glucose. Earth-abundant seawater was also tested for $H_2O_2$ generation[58] as displayed in Figure 5c yielding 220.9 ± 4.06 μM $H_2O_2$ production in saturated NaCl aqueous phase, slightly lower than pure water. In summary, with the minimal effects of inorganic and organic matter established, PTFE-catalyzed $H_2O_2$ generation has promising application prospects in over a range of biological and environmental systems.


https://doi.org/10.1021/acs.est.3c07674
Environ. Sci. Technol. 2024, 58, 925−934

## ENVIRONMENTAL IMPLICATIONS

In summary, ultrasonic water−PTFE tribocatalysis displays great promise for ambient atmosphere $H_2O_2$ production with rates up to 24.8 mmol $g_{cat}^{-1}$ $h^{-1}$ at a dosage of 0.01 g/L PTFE, which is significantly higher than that of state-of-the-art piezocatalysts and photocatalysts. Our in-depth investigation indicates that recombination of •OH produced by water oxidation is the predominant pathway for $H_2O_2$ production. This operational simplicity suggests that the present approach may complement existing photochemical and electrochemical $H_2O_2$ syntheses in a practical and environmentally friendly manner. Ultrasonic water−PTFE tribocatalysis offers the compelling advantages: (1) dominant direct water oxidation mechanism with no need for low-solubility oxygen, (2) operation at room temperature, ambient atmosphere, and without sacrificial agents, (3) utility at wide ranges of pH, inorganic anions and cations, (4) utilizing earth-abundant resources (seawater), and (5) no complicated material synthesis or waste treatment processes.

## ASSOCIATED CONTENT

### Supporting Information

The Supporting Information is available free of charge at https://pubs.acs.org/doi/10.1021/acs.est.3c07674.

Standard curve of $H_2O_2$ at 400 nm (Figure S1). Reaction scheme and mass spectrum of 4-carboxyphenylboronic acid with $H_2O_2$ (Figure S2). Continued ultrasonic $H_2O_2$ generation by PTFE (Figure S3). pH change of the solution caused by PTFE (Figure S4). Original unprocessed data of total ion chromatogram and mass spectra (Figure S5). $H_2O_2$ production over PTFE at the present of 200 mM TBA (Figure S6). Effect of bubbling $O_2$ on $H_2O_2$ generation (Figure S7). $H_2$ generation in the water−PTFE tribocatalytic system in the Ar atmosphere (Figure S8). (PDF)

## AUTHOR INFORMATION


### Corresponding Authors

**Jie Ding** − *State Key Laboratory of Pollution Control and Resource Reuse, School of Environment, Nanjing University, Nanjing 210023, China*; Email: dingjie0966@126.com

**Chad D. Vecitis** − *John A. Paulson School of Engineering and Applied Sciences, Harvard University, Cambridge, Massachusetts 02138, United States*; orcid.org/0000-0001-8813-4967; Email: vecitis@seas.harvard.edu

**Guandao Gao** − *State Key Laboratory of Pollution Control and Resource Reuse, School of Environment and Research Center for Environmental Nanotechnology (ReCENT), Nanjing University, Nanjing 210023, China*; orcid.org/0000-0002-2200-1341; Email: gaoguandao@nju.edu.cn

### Authors

**Yanfeng Wang** − *School of Life and Environmental Sciences, Shaoxing University, Shaoxing 312000, China; State Key Laboratory of Pollution Control and Resource Reuse, School of Environment, Nanjing University, Nanjing 210023, China*

**Peiyun Wei** − *School of Life and Environmental Sciences, Shaoxing University, Shaoxing 312000, China; State Key Laboratory of Pollution Control and Resource Reuse, School of Environment, Nanjing University, Nanjing 210023, China*

**Zihan Shen** − *State Key Laboratory of Multiphase Complex Systems, Institute of Process Engineering, Chinese Academy of Sciences, Beijing 100190, China*; orcid.org/0000-0002-5368-8190

**Chao Wang** − *School of Chemistry and Chemical Engineering, Yangzhou University, Yangzhou 225002, China*; orcid.org/0000-0001-6418-0504

**Wenkai Zhang** − *State Key Laboratory of Pollution Control and Resource Reuse, School of Environment, Nanjing University, Nanjing 210023, China*

**Xin Jin** − *State Key Laboratory of Pollution Control and Resource Reuse, School of Environment, Nanjing University, Nanjing 210023, China*; orcid.org/0000-0002-0142-6076

Complete contact information is available at: https://pubs.acs.org/10.1021/acs.est.3c07674


### Notes

The authors declare no competing financial interest.

## ACKNOWLEDGMENTS

The work was financially supported by National Natural Science Foundation of China (22276092, 22306121), China Postdoctoral Science Foundation (2023M733059), State Key Laboratory of Pollution Control and Resource Reuse Foundation Scientific Research (PCRRF22026), Start-Up Fund of Shaoxing University (13011001002/203, 13011001002/204), and Natural Science Foundation of Shaoxing University (2022LG005). The numerical calculations in this paper have been done on the computing facilities in the High Performance Computing Center (HPCC) of Nanjing University.

## REFERENCES


(1) Teranishi, M.; Naya, S.-i.; Tada, H. In Situ Liquid Phase Synthesis of Hydrogen Peroxide from Molecular Oxygen Using Gold Nanoparticle-Loaded Titanium(IV) Dioxide Photocatalyst. *J. Am. Chem. Soc.* **2010**, *132*, 7850−7851.

(2) Siahrostami, S.; Verdaguer-Casadevall, A.; Karamad, M.; Deiana, D.; Malacrida, P.; Wickman, B.; Escudero-Escribano, M.; Paoli, E. A.; Frydendal, R.; Hansen, T. W.; Chorkendorff, I.; Stephens, I. E. L.; Rossmeisl, J. Enabling direct $H_2O_2$ production through rational electrocatalyst design. *Nat. Mater.* **2013**, *12*, 1137−1143.

(3) Ling, C.; Liu, X.; Li, H.; Wang, X.; Gu, H.; Wei, K.; Li, M.; Shi, Y.; Ben, H.; Zhan, G.; Liang, C.; Shen, W.; Li, Y.; Zhao, J.; Zhang, L. Atomic-Layered $Cu_5$ Nanoclusters on $FeS_2$ with Dual Catalytic Sites for Efficient and Selective $H_2O_2$ Activation. *Angew. Chem., Int. Ed.* **2022**, *61*, No. e202200670.

(4) Zhu, Q.; Fan, J. C.; Tao, Y.; Shang, H.; Xu, J. C.; Zhang, D. Q.; Li, G. S.; Li, H. X. Photo-coupled electrocatalytic oxygen reduction to hydrogen peroxide using metal-free CNT-threaded oxidized g-$C_3N_4$. *Energy Mater.* **2022**, *2*, No. 200029.

(5) Campos-Martin, J. M.; Blanco-Brieva, G.; Fierro, J. L. G. Hydrogen peroxide synthesis: An outlook beyond the anthraquinone process. *Angew. Chem., Int. Ed.* **2006**, *45*, 6962−6984.

(6) Kim, H. W.; Ross, M. B.; Kornienko, N.; Zhang, L.; Guo, J. H.; Yang, P. D.; McCloskey, B. D. Efficient hydrogen peroxide generation using reduced graphene oxide-based oxygen reduction electrocatalysts. *Nat. Catal.* **2018**, *1*, 282−290.

(7) Moon, G.-h.; Kim, W.; Bokare, A. D.; Sung, N.-e.; Choi, W. Solar production of $H_2O_2$ on reduced graphene oxide-$TiO_2$ hybrid photocatalysts consisting of earth-abundant elements only. *Energy & Environ. Sci.* **2014**, *7*, 4023−4028.

(8) Hou, H. L.; Zeng, X. K.; Zhang, X. W. Production of hydrogen peroxide by photocatalytic processes. *Angew. Chem., Int. Ed.* **2020**, *59*, 17356−17376.

(9) Shiraishi, Y.; Kanazawa, S.; Tsukamoto, D.; Shiro, A.; Sugano, Y.; Hirai, T. Selective hydrogen peroxide formation by titanium dioxide photocatalysis with benzylic alcohols and molecular oxygen in water. *ACS Catal.* **2013**, *3*, 2222−2227.
(10) Burek, B. O.; Bahnemann, D. W.; Bloh, J. Z. Modeling and optimization of the photocatalytic reduction of molecular oxygen to hydrogen peroxide over titanium dioxide. *ACS Catal.* **2019**, *9*, 25−37.
(11) Zhang, J. Z.; Zheng, L. H.; Wang, F.; Chen, C.; Wu, H. D.; Leghari, S. A. K.; Long, M. The critical role of furfural alcohol in photocatalytic $H_2O_2$ production on $TiO_2$. *Appl. Catal., B* **2020**, *269*, No. 118770.
(12) Shiraishi, Y.; Kanazawa, S.; Kofuji, Y.; Sakamoto, H.; Ichikawa, S.; Tanaka, S.; Hirai, T. Sunlight-driven hydrogen peroxide production from water and molecular oxygen by metal-free photocatalysts. *Angew. Chem., Int. Ed.* **2014**, *126*, 13672−13677.
(13) Yang, L. P.; Dong, G. H.; Jacobs, D. L.; Wang, Y. H.; Zang, L.; Wang, C. Y. Two-channel photocatalytic production of $H_2O_2$ over g-$C_3N_4$ nanosheets modified with perylene imides. *J. Catal.* **2017**, *352*, 274−281.
(14) Hou, W.-C.; Wang, Y.-S. Photocatalytic generation of $H_2O_2$ by graphene oxide in organic electron donor-free condition under sunlight. *ACS Sustain. Chem. Eng.* **2017**, *5*, 2994−3001.
(15) Zhang, Q. Z.; Zhou, M. H.; Ren, G. B.; Li, Y. W.; Li, Y. C.; Du, X. D. Highly efficient electrosynthesis of hydrogen peroxide on a superhydrophobic three-phase interface by natural air diffusion. *Nat. Commun.* **2020**, *11*, 1731.
(16) Xue, Y. D.; Wang, Y. T.; Pan, Z. H.; Sayama, K. Electrochemical and photoelectrochemical water oxidation for hydrogen peroxide production. *Angew. Chem., Int. Ed.* **2021**, *60*, 10469−10480.
(17) Shi, X. J.; Siahrostami, S.; Li, G. L.; Zhang, Y. R.; Chakthranont, P.; Studt, F.; Jaramillo, T. F.; Zheng, X. L.; Nørskov, J. K. Understanding activity trends in electrochemical water oxidation to form hydrogen peroxide. *Nat. Commun.* **2017**, *8*, 701.
(18) Baek, J.; Jin, Q.; Johnson, N. S.; Jiang, Y.; Ning, R.; Mehta, A.; Siahrostami, S.; Zheng, X. L. Discovery of $LaAlO_3$ as an efficient catalyst for two-electron water electrolysis towards hydrogen peroxide. *Nat. Commun.* **2022**, *13*, 7256.
(19) Shi, X. J.; Back, S.; Gill, T. M.; Siahrostami, S.; Zheng, X. L. Electrochemical synthesis of $H_2O_2$ by two-electron water oxidation reaction. *Chem.* **2021**, *7*, 38−63.
(20) Zhang, K.; Liu, J. L.; Wang, L. Y.; Jin, B. J.; Yang, X. F.; Zhang, S. L.; Park, J. H. Near-complete suppression of oxygen evolution for photoelectrochemical $H_2O$ oxidative $H_2O_2$ synthesis. *J. Am. Chem. Soc.* **2020**, *142*, 8641−8648.
(21) Izgorodin, A.; Izgorodina, E.; MacFarlane, D. R. Low overpotential water oxidation to hydrogen peroxide on a $MnO_x$ catalyst. *Energy & Environ. Sci.* **2012**, *5*, 9496−9501.
(22) Kelly, S. R.; Shi, X. J.; Back, S.; Vallez, L.; Park, S. Y.; Siahrostami, S.; Zheng, X. L.; Nørskov, J. K. ZnO as an active and selective catalyst for electrochemical water oxidation to hydrogen peroxide. *ACS Catal.* **2019**, *9*, 4593−4599.
(23) Fan, L.; Bai, X. W.; Xia, C.; Zhang, X.; Zhao, X. H.; Xia, Y.; Wu, Z. Y.; Lu, Y. Y.; Liu, Y. Y.; Wang, H. T. $CO_2$/carbonate-mediated electrochemical water oxidation to hydrogen peroxide. *Nat. Commun.* **2022**, *13*, 2668.
(24) Kubota, K.; Pang, Y. D.; Miura, A.; Ito, H. Redox reactions of small organic molecules using ball milling and piezoelectric materials. *Science* **2019**, *366*, 1500−1504.
(25) Yan, X. H.; Li, G.; Wang, Z. Y.; Yu, Z. C.; Wang, K. Y.; Wu, Y. C. Recent progress on piezoelectric materials for renewable energy conversion. *Nano Energy* **2020**, *77*, No. 105180.
(26) Liang, Z.; Yan, C.-F.; Rtimi, S.; Bandara, J. Piezoelectric materials for catalytic/photocatalytic removal of pollutants: Recent advances and outlook. *Appl. Catal., B* **2019**, *241*, 256−269.
(27) Wang, Z. M.; Berbille, A.; Feng, Y. W.; Li, S.; Zhu, L. P.; Tang, W.; Wang, Z. L. Contact-electro-catalysis for the degradation of organic pollutants using pristine dielectric powders. *Nat. Commun.* **2022**, *13*, 130.
(28) Zhan, F.; Wang, A. C.; Xu, L.; Lin, S. Q.; Shao, J. J.; Chen, X. Y.; Wang, Z. L. Electron transfer as a liquid droplet contacting a polymer surface. *ACS Nano* **2020**, *14*, 17565−17573.
(29) Loh, Z.-H.; Doumy, G.; Arnold, C.; Kjellsson, L.; Southworth, S. H.; Al Haddad, A.; Kumagai, Y.; Tu, M. F.; Ho, P. J.; March, A. M.; Schaller, R. D.; Bin Mohd Yusof, M. S.; Debnath, T.; Simon, M.; Welsch, R.; Inhester, L.; Khalili, K.; Nanda, K.; Krylov, A. I.; Moeller, S.; Coslovich, G.; Koralek, J.; Minitti, M. P.; Schlotter, W. F.; Rubensson, J.-E.; Santra, R.; Young, L. Observation of the fastest chemical processes in the radiolysis of water. *Science* **2020**, *367*, 179−182.
(30) Park, S. Y.; Abroshan, H.; Shi, X. J.; Jung, H. S.; Siahrostami, S.; Zheng, X. L. $CaSnO_3$: An electrocatalyst for two-electron water oxidation reaction to form $H_2O_2$. *ACS Energy Lett.* **2019**, *4*, 352−357.
(31) Delley, B. From molecules to solids with the $DMol^3$ approach. *J. Chem. Phys.* **2000**, *113*, 7756.
(32) Perdew, J. P.; Burke, K.; Ernzerhof, M. Generalized Gradient Approximation Made Simple. *Phys. Rev. Lett.* **1996**, *77*, 3865−3868.
(33) Delley, B. An all-electron numerical method for solving the local density functional for polyatomic molecules. *J. Chem. Phys.* **1990**, *92*, 508−517.
(34) Dolg, M.; Wedig, U.; Stoll, H.; Preuss, H. Energy-adjusted *ab initio* pseudopotentials for the first row transition elements. *J. Chem. Phys.* **1987**, *86*, 866−872.
(35) Bergner, A.; Dolg, M.; Küchle, W.; Stoll, H.; Preuß, H. *Ab initio* energy-adjusted pseudopotentials for elements of groups 13−17. *Mol. Phys.* **1993**, *80*, 1431−1441.
(36) Lee, J. K.; Han, H. S.; Chaikasetsin, S.; Marron, D. P.; Waymouth, R. M.; Prinz, F. B.; Zare, R. N. Condensing water vapor to droplets generates hydrogen peroxide. *Proc. Natl. Acad. Sci. U.S.A.* **2020**, *117*, 30934−30941.
(37) Lee, J. K.; Walker, K. L.; Han, H. S.; Kang, J.; Prinz, F. B.; Waymouth, R. M.; Nam, H. G.; Zare, R. N. Spontaneous generation of hydrogen peroxide from aqueous microdroplets. *Proc. Natl. Acad. Sci. U.S.A.* **2019**, *116*, 19294−19298.
(38) Sellers, R. M. Spectrophotometric determination of hydrogen peroxide using potassium titanium (IV) oxalate. *Analyst* **1980**, *105*, 950−954.
(39) Waldo, N. B.; Vecitis, C. D. Combined effects of phase-shift and power distribution on efficiency of dual high-frequency sonochemistry. *Ultrason. Sonochem.* **2018**, *41*, 100−108.
(40) Hoffman, A. J.; Carraway, E. R.; Hoffmann, M. R. Photocatalytic production of $H_2O_2$ and organic peroxides on quantum-sized semiconductor colloids. *Environ. Sci. Technol.* **1994**, *28*, 776−785.
(41) Berbille, A.; Li, X. F.; Su, Y. S.; Li, S. N.; Zhao, X.; Zhu, L. P.; Wang, Z. L. Mechanism for Generating $H_2O_2$ at Water-Solid Interface by Contact-Electrification. *Adv. Mater.* **2023**, *35*, No. 2304387.
(42) Liu, J. L.; Zou, Y. S.; Jin, B. J.; Zhang, K.; Park, J. H. Hydrogen peroxide production from solar water oxidation. *ACS Energy Lett.* **2019**, *4*, 3018−3027.
(43) Perry, S. C.; Pangotra, D.; Vieira, L.; Csepei, L.-I.; Sieber, V.; Wang, L.; Ponce de Leon, C.; Walsh, F. C. Electrochemical synthesis of hydrogen peroxide from water and oxygen. *Nat. Rev. Chem.* **2019**, *3*, 442−458.
(44) Lindsey, M. E.; Tarr, M. A. Quantitation of hydroxyl radical during Fenton oxidation following a single addition of iron and peroxide. *Chemosphere* **2000**, *41*, 409−417.
(45) Zhou, L.; Feng, J. R.; Qiu, B. C.; Zhou, Y.; Lei, J. Y.; Xing, M. Y.; Wang, L. Z.; Zhou, Y. B.; Liu, Y. D.; Zhang, J. L. Ultrathin g-$C_3N_4$ nanosheet with hierarchical pores and desirable energy band for highly efficient $H_2O_2$ production. *Appl. Catal., B* **2020**, *267*, No. 118396.
(46) Lei, H.; Wu, M. X.; Mo, F.; Ji, S. L.; Dong, X. P.; Wu, Z.; Gao, J.; Yang, Y.; Jia, Y. M. Tribo-catalytic degradation of organic pollutants through bismuth oxyiodate triboelectrically harvesting mechanical energy. *Nano Energy* **2020**, *78*, No. 105290.
(47) Xu, W. H.; Zheng, H. X.; Liu, Y.; Zhou, X. F.; Zhang, C.; Song, Y. X.; Deng, X.; Leung, M.; Yang, Z. B.; Xu, R. X.; Wang, Z. L.; Zeng,


https://doi.org/10.1021/acs.est.3c07674
*Environ. Sci. Technol.* 2024, 58, 925−934

X. C.; Wang, Z. K. A droplet-based electricity generator with high instantaneous power density. *Nature* **2020**, *578*, 392−396.
(48) Zhao, J.; Zhang, X.; Xu, J.; Tang, W.; Lin Wang, Z.; Ru Fan, F. Contact-electro-catalysis for direct synthesis of $H_2O_2$ under ambient conditions. *Angew. Chem., Int. Ed.* **2023**, *62*, No. e202300604.
(49) Zhang, X. M.; Li, F.; Wang, C. H.; Guo, J. Z.; Mo, R. Y.; Hu, J.; Chen, S.; He, J. X.; Liu, H. H. Radial oscillation and translational motion of a gas bubble in a micro-cavity. *Ultrason. Sonochem.* **2022**, *84*, No. 105957.
(50) Xu, C.; Zi, Y. L.; Wang, A. C.; Zou, H. Y.; Dai, Y. J.; He, X.; Wang, P. H.; Wang, Y. C.; Feng, P. Z.; Li, D. W.; Wang, Z. L. On the electron-transfer mechanism in the contact-electrification effect. *Adv. Mater.* **2018**, *30*, No. 1706790.
(51) Gauduel, Y.; Pommeret, S.; Migus, A.; Antonetti, A. Some evidence of ultrafast $H_2O^+$-water molecule reaction in femtosecond photoionization of pure liquid water: Influence on geminate pair recombination dynamics. *Chem. Phys.* **1990**, *149*, 1−10.
(52) Chen, B. C.; Xia, Y.; He, R. X.; Sang, H. Q.; Zhang, W. C.; Li, J.; Chen, L. F.; Wang, P.; Guo, S. S.; Yin, Y. G.; Hu, L. G.; Song, M. Y.; Liang, Y.; Wang, Y. W.; Jiang, G. B.; Zare, R. N. Water−solid contact electrification causes hydrogen peroxide production from hydroxyl radical recombination in sprayed microdroplets. *Proc. Natl. Acad. Sci. U.S.A.* **2022**, *119*, No. e2209056119.
(53) Lacks, D. J; Mohan Sankaran, R Contact electrification of insulating materials. *J. Phys. D: Appl. Phys.* **2011**, *44*, No. 453001.
(54) Lowell, J.; Roseinnes, A. C. Contact electrification. *Adv. Phys.* **1980**, *29*, 947−1023.
(55) Chen, H.-Y. Why the reactive oxygen species of the Fenton reaction switches from oxoiron (IV) species to hydroxyl radical in phosphate buffer solutions? A computational rationale. *ACS omega* **2019**, *4*, 14105−14113.
(56) Khuntia, S.; Majumder, S. K.; Ghosh, P. Quantitative prediction of generation of hydroxyl radicals from ozone microbubbles. *Chem. Eng. Res. Des.* **2015**, *98*, 231−239.
(57) Nie, J. H.; Ren, Z. W.; Xu, L.; Lin, S. Q.; Zhan, F.; Chen, X. Y.; Wang, Z. L. Probing contact-electrification-induced electron and ion transfers at a liquid-solid interface. *Adv. Mater.* **2020**, *32*, No. 1905696.
(58) Mase, K.; Yoneda, M.; Yamada, Y.; Fukuzumi, S. Seawater usable for production and consumption of hydrogen peroxide as a solar fuel. *Nat. Commun.* **2016**, *7*, 11470.




https://doi.org/10.1021/acs.est.3c07674
*Environ. Sci. Technol.* 2024, 58, 925−934